Influence of thermal radiation on non-Darcian natural convection in a square cavity filled with fluid saturated porous medium of uniform porosity

Tapas Ray Mahapatra[a1], **Dulal Pal**[a], **Sabyasachi Mondal**[b]

[a]Department of Mathematics, Visva-Bharati (A Central University)
Santiniketan, West Bengal-731 235, India
trmahapatra@yahoo.com; dulalp123@rediffmail.com

[b]Bengal Institute of Technology and Management
Santiniketan, West Bengal-731 236, India
sabya.mondal.2007@gmail.com

Received: 3 April 2011 / **Revised:** 16 March 2012 / **Published online:** 21 May 2012

Abstract. Influence of thermal radiation on natural-convection flow in a square cavity filled with a porous medium of uniform porosity having isothermal vertical walls and adiabatic horizontal walls, has been studied numerically by using finite-difference method with staggered grid distribution. The simulation is performed by considering both Darcian and non-Darcian models. Governing momentum and energy equations are solved numerically to obtain velocity and temperature fields for various values of different physical parameters. It is seen that increasing the thermal radiation parameter enhances the local Nusselt number on the left vertical wall whereas the reverse effects are observed due to increase in the heat generating parameter when $Ra = 10^9$. The temperature at the mid-horizontal plane decreases with increase in the value of Rayleigh number up to a certain distance from the left vertical wall and beyond that distance the opposite trend is observed. The temperature at the mid-horizontal plane increases with increase in the value of heat generating parameter.

Keywords: natural convection, square cavity, Darcy–Forchheimer model, thermal radiation, heat generation.

1 Introduction

Studies on combined natural and forced convection have received a great attention due to its importance in practical applications in various modern systems such as electronic cooling, nuclear reactors, building management and solar energy systems. Natural convection flows are however particularly complex as they depend on several parameters among which the geometry and thermophysical characteristics of the fluid are the most important. A porous medium consists of a solid matrix with an interconnected void which

[1]Corresponding author.

is either rigid or deformable. Energy is transported through the porous materials in the underground such as sand and crushed rock saturated with water under the influence of local pressure gradients. The non-Darcy effects on natural convection in porous media have received a great deal of attention in the recent times due to numerous of technical applications associated with it, such as fluid flow in geothermal reservoirs, separation processes in chemical industries, solidification of casting, thermal insulation, petroleum reservoir, and so on. Walker and Homsy [1] and Bejan [2] used the assumption of a constant porosity porous medium based on Darcy's model. In order to account for the transition from Darcy flow to highly viscous flow at high permeability values, Brinkman [3] introduced Brinkman-extended Darcy model. However, this model does not provide adequate description for the transition from the porous medium flow to pure fluid flow. A model that bridges the gap between the Darcy and Navier–Stokes equations is the Darcy–Forchheimer model developed by Vafai and Tien [4]. In addition, Darcy–Brinkman–Forchheimer model describes the effects of inertia and viscous forces in the porous media as used by Poulikakos and Bejan [5] and Lauriat and Prasad [6]. Prasad and Tuntome [7] examined inertia effects on buoyancy driven flow and heat transfer in a vertical porous cavity using the Forchheimer-extended Darcy equation of motion for flow through porous media. Basak et al. [8] have investigated a natural convection flow in a square cavity filled with a porous medium for both uniform and non-uniform heating from below by using Darcy–Forchheimer model. Heat transfer due to natural convection in a cavity saturated with porous media is a new branch of thermo-fluid mechanics. The heat transfer phenomenon can be described by means of the hydrodynamics, the convective heat transfer mechanism and the electromagnetic field as they have a symbiotic relationship [9–11]. Effects of permeability and different thermal boundary conditions on the natural convection in a square cavity filled with porous media using Darcy–Forchheimer model were investigated by Saied and Pop [12], whereas Marcondes et al. [13] and Nithiarasu et al. [14] have considered Darcy–Brinkman–Forchheimer model in their study. The buoyancy effect on free convection in a vertical cavity was analyzed by Tong and Subramanian [15] and Lauriat and Prasad [16]. Li Tang et al. [17] studied combined heat and moisture convective transport in a partial enclosure with multiple free ports. Later Fu-Yun Zhao et al. [18] investigated free heat and mass transfer in a porous enclosure with side vents.

Two new dimensions are added in this study of natural convection flow in a cavity filled with porous medium by considering thermal radiation and internal heat source/sink effects. It is well known that the effect of thermal radiation is important in space technology and high temperature processes. Thermal radiation also plays an important role in controlling heat transfer process in polymer processing industry. The effect of radiation on heat transfer problems have been studied by Hossain and Takhar [19]. Later, Pal and Mondal [20] have investigated radiation effects on combined convection over a vertical flat plate embedded in a porous medium of variable porosity. In critical technological applications like in nuclear reactor cooling, the reactor bed can be modelled as a heat generating porous medium, quenched by a convective flow. Reddy and Narasimhan [21] studied the heat generation effects on natural convection inside a porous annulus. Although there are very few works in the field of natural convection cavity flow in presence

of thermal radiation parameter, still the works of Zahmatkesh [22] and Devika et al. [23] have helped a lot in this work. Zahmatkesh [22] has found that the presence of thermal radiation makes temperature distribution nearly uniform in the vertical sections inside the enclosure and causes the streamlines to be nearly parallel with the vertical walls. Devika et al. [23] has investigated the effect of radiation on non-Darcy convection heat transfer flow of a viscous electrically conducting fluid through a porous medium in a vertical channel.

The aim of the present work is to study the influence of thermal radiation and heat on natural convection flow in a square cavity filled with a fluid-saturated porous medium with isothermal vertical walls and adiabatic horizontal walls by considering Darcy–Brinkman–Forchheimer model. The governing equations are discretized, using finite-difference method with staggered grid formulation following MAC method proposed by Harlow and Welch [24]. The Poisson equation for pressure is derived using momentum and continuity equations and solved by BiCGStab method. The numerical results for streamline, isotherms, velocity, temperature profiles and the heat transfer rate at the heated walls in terms of local Nusselt number and average Nusselt number are presented.

2 Governing equations and boundary conditions

We consider natural convection heat transfer in an incompressible fluid in a square cavity of side length L filled with sparsely packed porous medium in the presence of thermal radiation and heat source/sink effects. The Rosseland approximation is used to describe the radiative heat flux in the energy equation. The radiative heat flux in the x-direction is considered negligible in comparison to the y-direction. Here the cavity filled with porous medium of uniform porosity has isothermal vertical walls and adiabatic horizontal walls. The geometry of this cavity together with the boundary conditions are illustrated in Fig. 1.

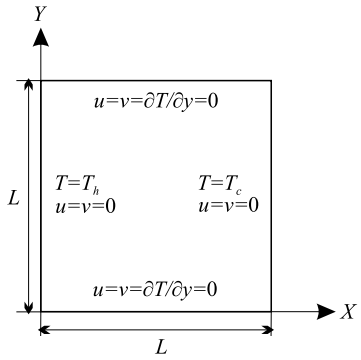

Fig. 1. Geometry and boundary conditions of the problem.

In the Cartesian coordinate system, the fundamental governing equations are as follows:

$$\frac{\partial U}{\partial X} + \frac{\partial V}{\partial Y} = 0, \tag{1}$$

$$\frac{\partial U}{\partial t'} + \frac{U}{\epsilon}\frac{\partial U}{\partial X} + \frac{V}{\epsilon}\frac{\partial U}{\partial Y} = -\frac{1}{\rho}\frac{\partial P}{\partial X} + \nu\left(\frac{\partial^2 U}{\partial X^2} + \frac{\partial^2 U}{\partial Y^2}\right) - \frac{\nu\epsilon}{K}U - \frac{1.75\sqrt{U^2+V^2}}{\sqrt{150K\epsilon}}U, \tag{2}$$

$$\frac{\partial V}{\partial t'} + \frac{U}{\epsilon}\frac{\partial V}{\partial X} + \frac{V}{\epsilon}\frac{\partial V}{\partial Y} = -\frac{1}{\rho}\frac{\partial P}{\partial Y} + \nu\left(\frac{\partial^2 V}{\partial X^2} + \frac{\partial^2 V}{\partial Y^2}\right) - \frac{\nu\epsilon}{K}V - \frac{1.75\sqrt{U^2+V^2}}{\sqrt{150K\epsilon}}V + g\beta(T-T_c), \tag{3}$$

$$\frac{\partial T}{\partial t'} + U\frac{\partial T}{\partial X} + V\frac{\partial T}{\partial Y} = \alpha\left(\frac{\partial^2 T}{\partial X^2} + \frac{\partial^2 T}{\partial Y^2}\right) - \frac{1}{\rho C_p}\frac{\partial q_r}{\partial Y} + \frac{Q}{\rho C_p}(T-T_c). \tag{4}$$

The associated boundary conditions are

$$\begin{aligned} &U(X,0) = U(X,L) = U(0,Y) = U(L,Y) = 0,\\ &V(X,0) = V(X,L) = V(0,Y) = V(L,Y) = 0,\\ &\frac{\partial T}{\partial Y}(X,0) = \frac{\partial T}{\partial Y}(X,L) = 0, \quad T(0,Y) = T_h \quad \text{and} \quad T(L,Y) = T_c. \end{aligned}$$

We now introduce dimensionless parameters given as follows:

$$\begin{aligned} &x = \frac{X}{L}, \quad y = \frac{Y}{L}, \quad u = \frac{UL}{\alpha}, \quad v = \frac{VL}{\alpha}, \quad \theta = \frac{T-T_c}{T_h-T_c},\\ &\alpha = \frac{\kappa}{\rho C_p}, \quad t = \frac{\alpha t'}{L^2}, \quad p = \frac{PL^2}{\rho\alpha^2}, \quad P_r = \frac{\nu}{\alpha}, \quad Da = \frac{K}{L^2},\\ &Ra = \frac{g\beta(T_h-T_c)}{\nu\alpha}L^3, \quad N_R = \frac{\kappa k^*}{4\sigma T_c^3}, \quad He = \frac{QL^2}{\kappa}. \end{aligned} \tag{5}$$

Here g, κ, C_p and Q denote acceleration due to gravity, thermal conductivity, specific heat at constant pressure and heat generation constant respectively. t', T, T_h and T_c indicate time, fluid temperature, temperature of the hot wall and temperature of the cold wall (the reference temperature), respectively. Here α, ρ, ν, μ and Da denote thermal diffusivity, density, kinematic viscosity, dynamic viscosity of the fluid and the Darcy number respectively. L is an appropriate macroscopic length scale that can be used to relate flow in a porous medium with flow in a clear fluid. ϵ, Ra, N_R and He are the porosity of the porous medium, Rayleigh number, thermal radiation parameter and heat generation/absorption parameter, respectively. Here K denotes permeability of the porous medium and the radiation heat flux q_r is considered according to Rosseland approximation such that $q_r = -(4\sigma)/(3k^*)(\partial T^4)/(\partial Y)$, where σ and k^* are the Stefan–Boltzmann constant and the mean absorption coefficient, respectively. Following Raptis [25], the fluid-phase temperature differences within the flow are assumed to be sufficiently small so that T^4 may be expressed as a linear function of temperature. This is done by expanding T^4 in a Taylor series about the temperature T_c and neglecting higher order terms to yield, $T^4 \cong 4T_c^3T - 3T_c^4$ [22].

Using dimensionless quantities given by Eqs. (5), we obtain the following dimensionless governing equations:

$$\frac{\partial u}{\partial x}+\frac{\partial v}{\partial y}=0, \tag{6}$$

$$\frac{\partial u}{\partial t}=-\frac{\partial p}{\partial x}+Pr\left(\frac{\partial^2 u}{\partial x^2}+\frac{\partial^2 u}{\partial y^2}\right)-\frac{1}{\epsilon}\left(\frac{\partial u^2}{\partial x}+\frac{\partial uv}{\partial y}\right)-\frac{Pr\epsilon}{Da}u -\frac{1.75\sqrt{u^2+v^2}}{\sqrt{150Da\epsilon}}u, \tag{7}$$

$$\frac{\partial v}{\partial t}=-\frac{\partial p}{\partial y}+Pr\left(\frac{\partial^2 v}{\partial x^2}+\frac{\partial^2 v}{\partial y^2}\right)-\frac{1}{\epsilon}\left(\frac{\partial v^2}{\partial y}+\frac{\partial uv}{\partial x}\right)-\frac{Pr\epsilon}{Da}v -\frac{1.75\sqrt{u^2+v^2}}{\sqrt{150Da\epsilon}}v+PrRa\epsilon\theta, \tag{8}$$

$$\frac{\partial \theta}{\partial t}=\left(\frac{\partial^2\theta}{\partial x^2}+\frac{\partial^2\theta}{\partial y^2}\right)-\left(\frac{\partial u\theta}{\partial x}+\frac{\partial v\theta}{\partial y}\right)+\frac{4}{3N_R}\frac{\partial^2\theta}{\partial y^2}+He\,\theta. \tag{9}$$

The dimensionless boundary condition are

$$\begin{aligned}&u=v=\frac{\partial\theta}{\partial y}=0 \quad \text{at } y=0,\ y=1,\\ &u=v=0 \quad \text{at } x=0,\ x=1,\\ &\theta=1 \quad \text{at } x=0 \quad \text{and} \quad \theta=0 \quad \text{at } x=1.\end{aligned}$$

The heat transfer coefficient in terms of the local Nusselt number (Nu) is $Nu = -(\partial\theta)/(\partial n)$, where n denotes the normal direction to a plane. The local Nusselt number at the left vertical wall (Nu_l) is $Nu_l = -(\partial\theta)/(\partial x)|_{x=0}$. The average Nusselt number at the hot wall is $\overline{Nu}_H = \int_0^1 Nu\,\mathrm{d}y$. The relationships between stream function, ψ and velocity components for two-dimensional flows are $u = \partial\psi/\partial y$, $v = -(\partial\psi)/(\partial x)$. From this definition of stream function, the positive sign of ψ denotes anti-clockwise circulation and the clockwise circulation is represented by the negative sign of ψ. The governing equations from (6)–(9) in absence of radiation and heat generation parameters of the generalized model in the non-Darcian regime are same with Medeiros et al. [32].

3 Method of solution

Some computer codes related to heat transfer using staggered grid were developed by Patankar and Spalding [26], Patankar [27], Amsden and Harlow [28], Hirt et al. [29], Van Doormal and Raithby [30] which are well known in the literature. In the present work, control-volume based finite-difference discretization of the non-dimensional governing equations are carried out in a staggered grid, popularity known as MAC cell [24]. The derivatives involved in convective terms are discretized using a hybrid scheme which is

a convex combination of second-order central-difference and second-order upwind difference scheme. But the derivatives involved in other terms are discretized using second-order central-difference scheme. The pressure Poisson equation is derived from the discretized momentum and continuity equations. We now describe the iteration process to obtain the solutions of the basic equations with appropriate boundary conditions. In the derivation of pressure Poisson equation, the divergence term at nth time level $(D^n_{i\,j})$ is retained and evaluated in the pressure Poisson iteration. It is done because the discretized form of divergence of velocity field, i.e., D^n_{ij} is not guaranteed to be zero. The solution procedure starts with the initializing the velocity field. This is done either from the result of previous cycle or from the prescribed initial and boundary conditions. Using this velocity field, pressure Poisson equation is solved using BiCGStab method. Knowing pressure field, the u-momentum, v-momentum and temperature equations are solved and the values of u, v, θ are updated to get the values at $(n+1)$th time level. Using the values of u and v at $(n+1)$th time level, the value of the divergence of velocity field is checked for its limit. If its absolute value is less than 0.5×10^{-5} and steady state reaches then iteration process stops, otherwise pressure Poisson equation is solved again for pressure.

4 Numerical stability criteria

Linear stability of fluid flow is $\delta t_1 \leq \min[\frac{\delta x}{|u|}, \frac{\delta y}{|v|}]$, which is related to convection of fluid, i.e., fluid should not move more than one cell width per time step (Courant, Friedrichs and Lewy condition). Also, from the Hirt's stability analysis, $\delta t_2 \leq \min[\frac{1}{2Pr}\frac{\delta x^2 \delta y^2}{(\delta x^2+\delta y^2)}]$. This condition roughly stated that momentum cannot diffuse more than one cell width per time step. The time step actually used in the computations is determined from $\delta t = FCT \times [\min(\delta t_1, \delta t_2)]$, where the factor FCT varies from 0.2 to 0.4. The upwinding parameter β is governed by the inequality condition $1 \geq \beta \geq \max[|\frac{u\delta t}{\delta x}|, |\frac{v\delta t}{\delta y}|]$. As a rule of thumb, β is taken approximately 1.2 times larger than what is found from the above inequality condition.

5 Results and discussions

In this study, numerical results are obtained for natural convection flow in unit square cavity for grid size (80×80) with uniform porosity ($\epsilon = 0.4$) and different Rayleigh number Ra, ($10^8 \leq Ra \leq 5 \times 10^9$), Darcy number Da, ($10^{-6} \leq Da \leq 10^{-2}$), thermal radiation parameter N_R, ($0.0 \leq N_R \leq 10.0$), heat generating parameter He, ($0.0 \leq He \leq 10.0$), Prandtl number Pr, ($0.7 \leq Pr \leq 7.0$) which are illustrated through several tables and figures. Grid independence test is provided in Table 1 for various grid size. It is important to note that as the number of grid points are increased there is drastically increase in the number of iterations to get the converged results for $|\psi_{\min}|$. But when the number of grid points is increases from 80×80 to 160×160, there is no significant change found in the value of $|\psi_{\min}|$. Hence, all the results are computed with 80×80 grid points.

Table 1. Grid independence test in absence of radiation and heat generation parameters when $Pr = 1.0$, $Ra = 10^8$, $Da = 10^{-4}$ and $\epsilon = 0.4$.

No. of grid points	Iteration	$\lvert\psi_{\min}\rvert$
20×20	32369	26.5700
40×40	81095	28.3138
80×80	169090	28.4806
160×160	346823	27.7136

In Table 2 values of $\overline{Nu}_H|_{x=0}$ are computed for Darcy, non-Darcy and non-porous models for different values of Ra and N_R. It is observed from this table that the values of $\overline{Nu}_H|_{x=0}$ for non-porous model is higher than those of Darcy and non-Darcy models. Thus it is useful to include thermal radiation effects in the study of natural convection in a square cavity with uniform porosity. Further, it is observed that the non-porous model is effective for all the values of thermal radiations parameter and Rayleigh number. It is observed that $\overline{Nu}_H|_{x=0}$ values are also higher for non-porous model than non-Darcy model and Darcy model for both of $Ra = 10^8$ and 10^9.

Table 2. Computed values of $\overline{Nu}_H|_{x=0}$ when $He = 0.2$ for various values of Ra and N_R.

Ra	N_R	$\overline{Nu}_H\|_{x=0} \rightarrow$		
		Darcy model $Da = 10^{-6}, \epsilon = 0.4$	non-Darcy model $Da = 10^{-6}, \epsilon = 0.4$	non-porous
10^8	0.5	2.2946	2.3129	34.0726
	1.0	2.5604	2.5817	34.6553
	5.0	2.9046	2.9298	35.1909
	10.0	2.9623	2.9881	35.2642
10^9	0.5	10.5798	11.4722	60.4263
	1.0	11.2802	12.2260	60.9234
	5.0	11.9901	12.9798	61.3493
	10.0	12.0909	13.0857	61.4045

Comparison of the average Nusselt number at the hot wall ($x = 0$) for a non-Darcian regime with uniform porosity is made with Nithiarasu et al. [31] and Medeiros et al. [32] for various values of Rayleigh number Ra in Table 3. It is noted from this table that an average Nusselt number increases with increase in the value of Rayleigh number Ra.

Table 4 presents the computed values of the average Nusselt number ($\overline{Nu}_H|_{x=0}$) at the hot wall ($x = 0$) with uniform porosity ($\epsilon = 0.4$) for various values of radiation parameter N_R, heat generating parameter He, and Rayleigh number Ra. From this table it is seen that when radiation parameter N_R increases from 0.5 to 10.0, the average Nusselt number increases. It is also observed from this table that the average Nusselt number decreases with increasing heat generating parameter He and the average Nusselt number increases when Rayleigh number Ra increases.

Table 5 shows the computed values of the average Nusselt number ($\overline{Nu}_H|_{x=0}$) at the hot wall ($x = 0$) with uniform porosity for various values of Rayleigh number and Prandtl number. It is observed from this table that the average Nusselt number increases

with increasing Pr keeping other parameter fixed. It is also seen that as Ra increases the difference of average Nusselt number increases between the Prandtl numbers.

Table 3. Comparison of average Nusselt number $\overline{Nu}_H|_{x=0}$ in absence of radiation and heat generation parameters of the generalized model in the non-Darcian regime, when $Pr = 1$, $Da = 10^{-6}$, $\epsilon = 0.4$.

Ra	$\overline{Nu}_H\|_{x=0}$		
	Nithiarasu et al. [31]	Medeiros et al. [32]	Present work
10^8	2.97	3.05	3.07
10^9	11.46	12.10	12.23
5×10^9	23.09	24.74	24.43

Table 4. Computed values of $\overline{Nu}_H|_{x=0}$ when $Pr = 1$, $Da = 10^{-6}$ and $\epsilon = 0.4$ for various values of Ra, N_R and He.

Ra	He	N_R	$\overline{Nu}_H\|_{x=0}$
10^8	0.2	0.5	2.29
		1.0	2.56
		5.0	2.90
		10.0	2.96
10^8	0.5	1.0	2.58
	1.0		2.34
	5.0		1.10
	10.0		−1.00
10^6	0.2	1.0	0.93
10^7			0.99
10^8			2.56
10^9			11.28

Table 5. Computed values of $\overline{Nu}_H|_{x=0}$ when $Da = 10^{-6}$, $N_R = 1.0$, $He = 1.0$ and $\epsilon = 0.4$ for various values of Ra and Pr.

Ra	Pr	$\overline{Nu}_H\|_{x=0}$
10^7	0.7	0.4212
	1.0	0.4214
	7.0	0.4215
10^8	0.7	2.3369
	1.0	2.3458
	7.0	2.3641
10^9	0.7	10.8246
	1.0	11.1171
	7.0	11.8845

Figures 2(a), 2(b) show the velocity and temperature profiles, respectively, at the mid-horizontal plane for $Pr = 1$, $Da = 10^{-6}$, $He = 0.2$ and for two values of Ra i.e., Ra=10^8, 10^9. It is observed from these two figures that when the value of thermal radiation N_R is increased then the vertical velocity profiles and temperature profiles do not show any appreciable change for both $Ra = 10^8$, 10^9. Further, it is observed that the vertical velocity profile increases with increase in the value of the Rayleigh number, Ra, with increase in the formation of the peak near the left vertical wall, whereas reverse effect is observed at the right vertical wall as seen from Fig. 2(a). It is to be pointed out that in the case of temperature profiles, the Rayleigh number plays an important role in enhancing the temperature with decrease in the value of Ra at the left vertical wall whereas opposite effect of Ra is seen at the right vertical wall as seen from Fig. 2(b).

The variation of vertical velocity profiles at the mid-horizontal plane of the cavity considering uniform porosity is depicted in Fig. 3(a) for various values of Ra and He for $Pr = 1$, $Da = 10^{-6}$, $N_R = 1$ and $\epsilon = 0.4$. It is thus observed that the effect of

increasing the value of He is to decrease the center line vertical velocity near the left vertical hot wall whereas reverse effect is observed near the right vertical wall for fixed value of Ra. Figure 3(b) depicts the effects of heat generation coefficient on temperature at the mid-horizontal plane of the cavity for $Pr = 1$, $Da = 10^{-6}$, $N_R = 1$ and $\epsilon = 0.4$ when $Ra = 10^8, 10^9$. It is seen that temperature at the mid horizontal plane increases with increase in He for both $Ra = 10^8$ and $Ra = 10^9$. It is well known that the heat generation causes the fluid temperature to increase which has a tendency to increase the thermal buoyancy effects. These effects are clearly seen from this figure.

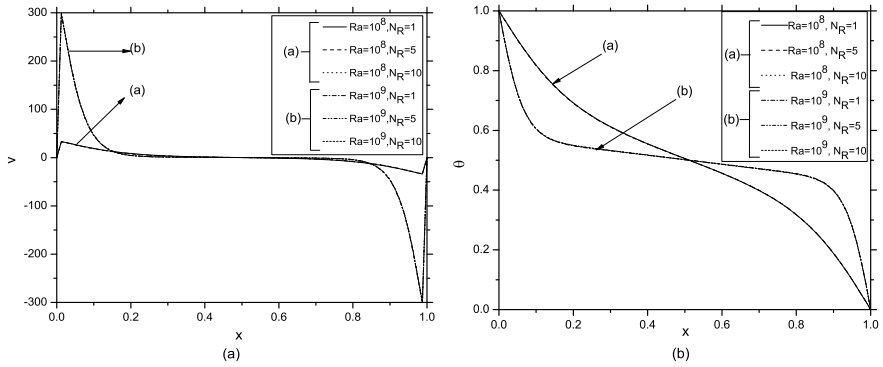

Fig. 2. (a) Vertical velocity profiles; (b) Temperature profiles at mid-horizontal plane for various values of Ra and N_R when $Pr = 1$, $Da = 10^{-6}$ and $He = 0.2$.

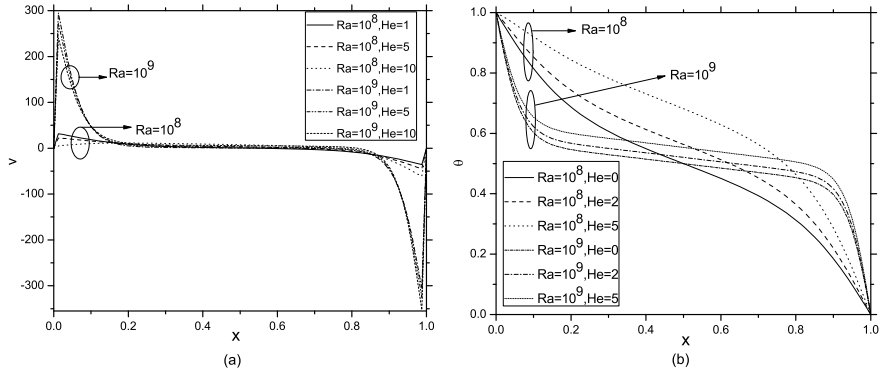

Fig. 3. (a) Vertical velocity profiles; (b) Temperature profiles at mid-horizontal plane for various values of Ra and He.

Figures 4(a) and 4(b) show the effects of Da on vertical velocity and temperature profiles at mid-horizontal plane when $Pr = 1$, $Ra = 10^8$, $N_R = 1$ and $He = 0.2$. From Fig. 4(a) we observe that the center line vertical v-velocity increases rapidly near the hot wall ($x = 0$) forming a peak and then decreases rapidly to arrive at the zero value

and remains so before reaching closer to the cold wall. In the neighbourhood region of the cold wall, the velocity rapidly falls to attain a negative peak value and then increases rapidly to match the boundary condition at the cold wall. It is also seen that the vertical velocity at mid-horizontal plane in the cavity filled with porous medium increases as Da increases near the hot wall and reverse effect is seen near the cold wall of the cavity. Peak value attained by center-line vertical velocity in the case of cavity without porous medium is much higher than that in case of cavity filled with porous medium. Figure 4(b) shows the temperature at the mid-horizontal plane in the presence and absence of the porous media. It is seen that the center-line temperature decreases as Da increases near the hot wall up to a certain value of x ($x = 0.5$) but beyond that distance opposite trend is observed near the cold wall of the cavity. It is also observed that for the cavity having no porous medium, the center-line temperature decreases sharply in the vicinity of hot wall and remains constant for long and thereafter it decreases sharply and reaches to zero at the right boundary wall. Further, it is observed from this figure that the center-line temperature profiles are concurrent for all the values of the Da.

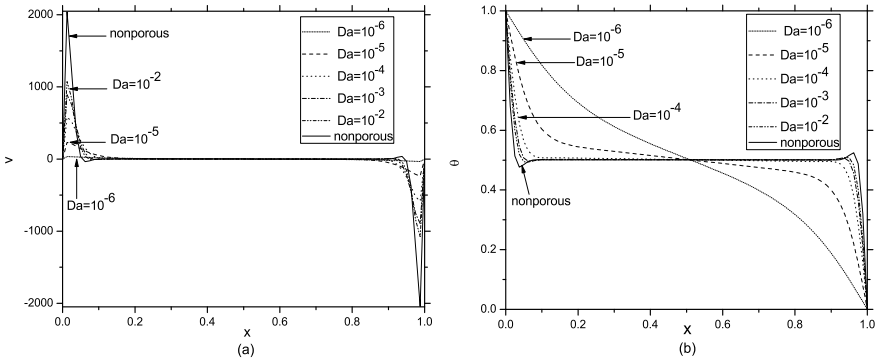

Fig. 4. (a) Vertical velocity profiles; (b) Temperature profiles at mid-horizontal plane for various values of Da.

The effect of Darcy number Da on the streamlines and isotherms are illustrated in Figs. 5, 6 for different values of $Da = 10^{-6}, 10^{-2}$ and $Ra = 10^8, 10^9$ for uniform heating of the left vertical wall. Due to heating of the left vertical wall, the fluid rise up along the sides of the hot vertical wall which flows towards the cold vertical wall, forming a clockwise eddy inside the cavity. Figure 5(a) depicts the streamlines and isotherms for $Da = 10^{-6}$ and $Ra = 10^8$. From this figure it is seen that the flow is very weak and hence the isotherms change very smoothly from the hot vertical wall to the cold vertical wall which shows that the heat transfer is dominated by the conduction. Now, when Fig. 5(a) is compared with Figs. 5(b), 6(a), it is observed that the streamlines and isotherms concentrated near the edges of left and right vertical walls due to stronger circulation, which results in higher heat transfer rate due to convection. The fluid circulation is strongly dependent on Da as can be seen from Figs. 5(a), (b) and 6(a). It is seen from Figs. 5(b) and 6(a) that the boundary layers are relatively thick and a very small core region occurs

such that the isotherms which become almost parallel to the horizontal walls indicating that the conduction regime is approached. Thus as the Da is increased, the intensity within the cavity increases due to reduced resistance offered from the porous medium. Thus higher permeability of the porous medium is significantly more important for the heat transfer rate. Figure 6(b) is the plot of the streamlines and isotherms for $Da = 10^{-6}$ and $Ra = 10^9$. A comparison of Fig. 5(a) and Fig. 6(b) reveals that as the value of Ra increases from 10^8 to 10^9 with $Da = 10^{-6}$, the buoyancy-driven circulation inside the cavity is also increased, as seen from the greater magnitudes of the stream functions. Further, it is observed that circulations are greater near the center and least at the wall. Thus, the temperature gradient near both the left and right vertical walls is significant in developing the thermal boundary layer.

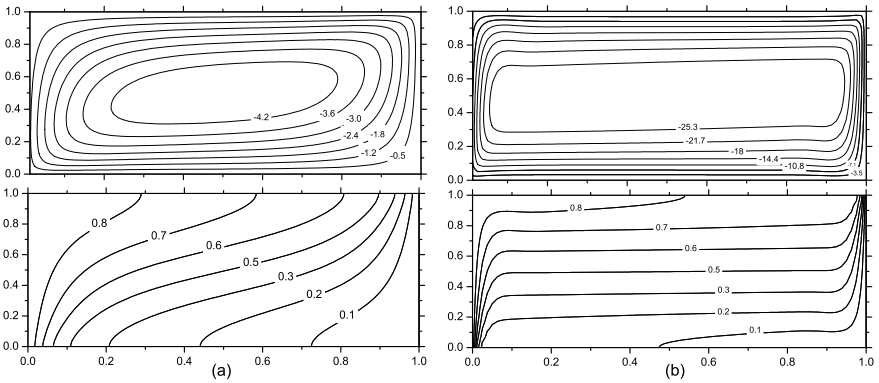

Fig. 5. Streamlines and isotherms for (a) $Da = 10^{-6}$, $Ra = 10^8$, $Pr = 1$, $N_R = 1$, $He = 0.2$ and (b) $Da = 10^{-4}$, $Ra = 10^8$, $Pr = 1$, $N_R = 1$ and $He = 0.2$.

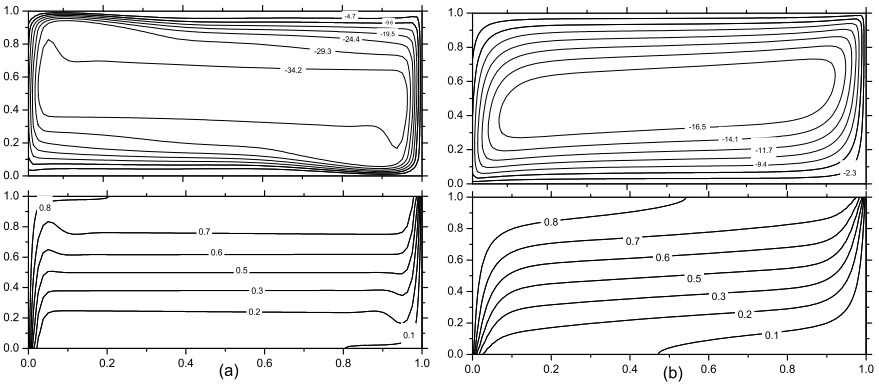

Fig. 6. Streamlines and isotherms for (a) $Da = 10^{-2}$, $Ra = 10^8$, $Pr = 1$, $N_R = 1$, $He = 0.2$ and (b) $Da = 10^{-6}$, $Ra = 10^9$, $Pr = 1$, $N_R = 1$ and $He = 0.2$.

The effects of the Rayleigh number Ra ($10^8 \leq Ra \leq 5 \times 10^9$) on the local Nusselt number at the left vertical wall in the absence of thermal radiation and heat generating parameters are displayed in Fig. 7(a). It is observed from this figure that the heat transfer rate increases when Rayleigh number increases. In the case of uniform heating, the heat transfer rate at the left vertical wall or Nu_l is very high at the left edge of the left vertical wall, due to the presence of discontinuity in the temperature boundary conditions at this edge. Further, the local heat transfer rate at the cold right vertical wall has its minimum value. The effects of thermal radiation on the heat transfer rates are displayed in Figs. 7(b), 8(a). From Figs. 7(b) and 8(a) it is seen that Nu_l increases when N_R increase up to a certain value of y ($y = 0.55$) but beyond which the opposite trend is observed. Figure 8(b) presents the variation of Nu_l with y for various values of Ra and He. It is observed from this figure that Nu_l decreases as He increases for both values of $Ra = 10^8$ and 10^9 but Nu_l increases as Ra increases from $Ra = 10^8$ to $Ra = 10^9$.

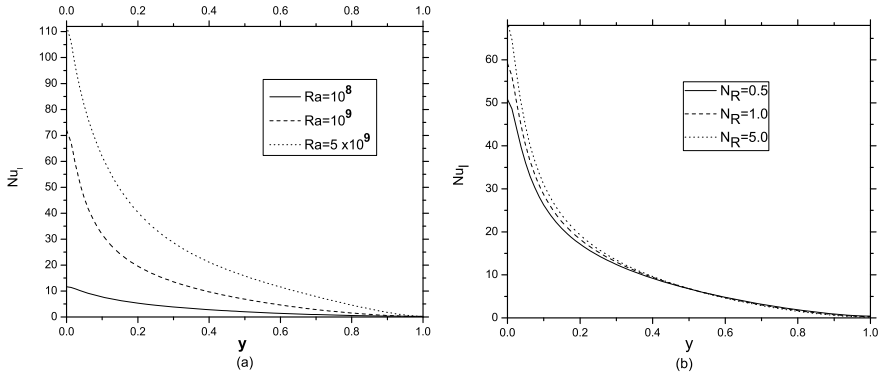

Fig. 7. Local Nusselt number at the left vertical wall for different values of (a) Ra when $Pr = 1$, $Da = 10^{-6}$, $N_R = He = 0$ and (b) N_R when $Pr = 1, Ra = 10^9$, $Da = 10^{-6}$ and $He = 0.2$.

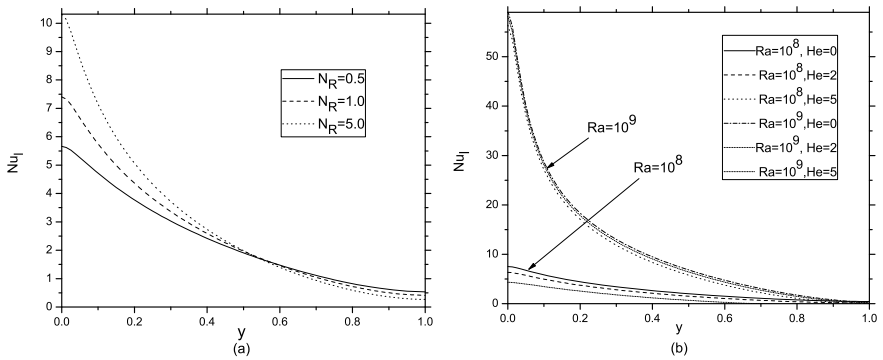

Fig. 8. Local Nusselt number at the left vertical wall for different values of (a) N_R when $Pr = 1$, $Ra = 10^8$, $Da = 10^{-6}$, $He = 0.2$ and (b) Ra and He when $Pr = 1$, $Da = 10^{-6}$, $N_R = 1$.

6 Conclusions

Influence of thermal radiation on non-Darcian natural convection in a square cavity filled with fluid saturated porous medium of uniform porosity is studied in the present paper. Results for the vertical velocity and temperature at the mid-horizontal plane of the cavity, local Nusselt number and average Nusselt number are obtained for representative governing physical parameters. Streamlines and isotherms for various values of Darcy number and Rayleigh number are shown graphically. As a summary, we conclude the following:

1. The effect of increasing the Rayleigh number is to enhance the vertical velocity at the mid-horizontal plane up to a certain distance from the left vertical wall and beyond that distance the opposite trend is observed.
2. The temperature at the mid-horizontal plane decreases with increase in the value of Rayleigh number up to a certain distance from the left vertical wall and beyond that distance the opposite trend is observed.
3. The effects of thermal radiation on velocity and temperature profiles are not very significant.
4. The vertical velocity at the mid-horizontal plane decreases with increasing the value of heat generating parameter near the left vertical wall whereas reverse effect is observed near the right vertical wall.
5. The temperature at the mid-horizontal plane increases with increase in the value of heat generating parameter.
6. The streamlines and isotherms concentrated near the walls and edges of left and right vertical walls due to stronger circulation, respectively.
7. Heat transfer rate at the left vertical wall is very high at the bottom side of the left vertical wall, due to the presence of discontinuity in the temperature boundary conditions and it has its minimum value at the upper side of the left vertical wall.
8. Average Nusselt number increases with increase in the thermal radiation parameter but reverse effect is observed when heat generating parameter increases.

Acknowledgments

One of the authors (Tapas Ray Mahapatra) acknowledges the financial support of partial research grant of Visva-Bharati, Santiniketan, India. The authors also thank the referees for their valuable comments which helped to improve the presentation of the paper.

References

1. K.L. Walker, G.M. Homsy, Convection in a porous cavity, *J. Fluid. Mech.*, **87**, pp. 449–474, 1978.

2. A. Bejan, On the boundary layer regime in a vertical enclosure filled with a prous medium, *Lett. Heat Mass Trans.*, **6**, pp. 93–102, 1979.

3. H.C. Brinkman, On the permeability of media consisting of closely packed porous particles, *Appl. Sci. Res.*, **1**, pp. 81–86, 1949.

4. K.E. Vafai, C.L. Tien, Boundary and inertia effects on flow and heat transfer in porous media, *Int. J. Heat Mass Transfer*, **24**, pp. 195–204, 1981.

5. D. Poulikakos, A. Bejan, The departure from Darcy flow in natural convection in a vertical porous layer, *Phys. Fluids*, **28**, pp. 3477–3484, 1985.

6. G. Lauriat, V. Prasad, Non-Darcian effects natural convection in a vertical porous enclosure, *Int. J. Heat Mass Transfer*, **32**, pp. 2135–2148, 1989.

7. V. Prasad, A. Tuntomo, Inertia effects on natural convection in a vertical porous cavity, *Numer. Heat Transfer*, **11**, pp. 295–320, 1987.

8. T. Basak, S. Roy, T. Paul, I. Pop, Natural convection in square cavity filled with a porous medium: Effects of various thermal boundary conditions, *Int. J. Heat Mass Transfer*, **49**, pp. 1430–1441, 2006.

9. D.A. Nield, A. Bejan, *Convection in Porous Media*, 3rd edition, Springer, New York, 2006.

10. K. Vafai, *Handbook of Porous Media*, 2nd edition, Taylor and Francis, Boca Raton, 2005.

11. P. Vadasz, *Emerging Topics in Heat and Mass Transfer in Porous Media*, Springer, New York, 2008.

12. N.H. Saied, I. Pop, Non-Darcy natural convection in a square cavity filled with a porous media, *Fluid Dyn. Res.*, **36**, pp. 35–43, 2005.

13. F. Marcondes, J.M. Mederios, J.M. Gurgel, Numerical analysis of natural convection in cavities with variable porosity, *Numer. Heat Transfer, Part A*, **40**, pp. 403–420, 2001.

14. P. Nithiarasu, K.N. Seetharamu, T. Sundararajan, Numerical investigation of buoyancy driven flow in a fluid saturated non-Darcian porous medium, *Int. J. Heat Mass Transfer*, **42**, pp. 1205–1215, 1999.

15. T.W. Tong, E. Subramanian, A boundary layer analysis for natural convection in vertical porous enclosures: Use of Brink-extended Darcy model, *Int. J. Heat Mass Transfer*, **28**, pp. 563–571, 1985.

16. G. Lauriat, V. Prasad, Natural convection in a vertical porous cavity: A numerical study for Brinkman-extended Darcy formulation, *J. Heat Transfer*, **109**, pp. 688–696, 1987.

17. L. Tang, D. Liu, F.-Y. Zhao, G.-F. Tang, Combined heat and moisture convective transport in a partial enclosure with multiple free ports, *Appl. Therm. Eng.*, **30**, pp. 977-990, 2010.

18. F.-Y. Zhao, D. Liu, H.-Q. Wang, G.-X. Kou, G.-F. Tang, Free heat and mass transfer in a porous enclosure with side vents, *Drying Technol.*, **29**, pp. 91-104, 2011.

19. M.A. Hossain, H.S. Takhar, Radiation effect on mixed convection along a vertical plate with uniform surface temperature, *Heat Mass Transfer*, **31**, pp. 243–248, 1996.

20. D. Pal, H. Mondal, Radiation effects on combined convection over a vertical flat plate embedded in a porous medium of variable porosity, *Meccanica*, **44**, pp. 133–144, 2009.

21. B.V.K. Reddy, A. Narasimhan, Heat generation effects in natural convection inside a porous annulus, *Int. Commun. Heat Mass Transfer*, **37**, pp. 607–610, 2010.

22. I. Zahmatkesh, Influence of thermal radiation on free convection inside a porous enclosure, *Emirates Journal for Engineering Research*, **12**(2), pp. 47–52, 2007.

23. R.B. Devika, P.V.B. Reddy, D.R.V.P. Rao, Effect of radiation on non-Darcy convective heat transfer through a porous medium in a vertical channel, *J. Comp. Math. Sci.*, **2**(3), pp. 483–492, 2011.

24. F.H. Harlow, J.E. Welch, Numerical calculation of time dependent viscous incompressible flow of fluid with free surface, *Phys. Fluids*, **25**, pp. 2182–2189, 1965.

25. A. Raptis, Radiation and free convection flow through a porous medium, *Int. Commun. Heat Mass Transfer*, **25**, pp. 289–295, 1998.

26. S.V. Patankar, D.B. Spalding, A calculation procedure for heat mass and momentum transfer in three-dimensional parabploicflows, *Int. J. Heat Mass Transfer*, **15**, pp. 1787–1806, 1972.

27. S.V. Patankar, *Numerical Heat Transfer and Fluid Flow*, McGraw-Hill, New York, 1980.

28. A.A. Amsden, F.H. Harlow, The SMAC method: A numerical technique for calculating incompressible fluid flow, Report LA-4370, Los Alamos Scientific Laboraty, 1970.

29. C.W. Hirt, B.D. Nichols, N.C. Romero, SOLA-A numerical solution algorithm for transient fluid flows, Report UC-34 and UC-79d, Los Alamos Scientific Laboraty, University of California, New Mexico, 1975.

30. J.P. Van Doormal, G.D. Raithby, Enhancement of the SIMPLE method for prediction incompressible fluid flow, *Numer. Heat Transfer*, **7**, pp. 147–163, 1984.

31. P. Nithiarasu, K.N. Seetharamu, T. Sundararajan, Natural convective heat transfer in a fluid saturated variable porosity medium, *Int. J. Heat Mass Transfer*, **40**, pp. 3955–3967, 1997.

32. J.M. Medeiros, F. Marcondes, J.M. Gurgel, Natural convection in a porous cavity using the generalized model with uniform porosity, in: *Proceedings of the 15th Brazilian Congress of Mechanical Engineering, XV COBEM*, Aguas de Lindoia, Sao Paulo, Brazil, 1999 (on CD-ROM).